


ARTICLE



FBXO38 regulates macrophage polarization to control the development of cancer and colitis

Xin Zheng^{1,2,3}, Qi Jiang^{1,3}, Mingshun Han², Fenfen Ye¹, Mingchang Wang², Ying Qiu², Jialu Wang¹, Minxia Gao², Fajian Hou^{1,2} and Hongyan Wang^{1,2} 

© The Author(s), under exclusive licence to CSI and USTC 2023

Macrophages are highly plastic cells that differentially regulate multiple pathological conditions, including cancer and autoimmune diseases. In response to various stimuli, macrophages activate different intrinsic signaling pathways and polarize into distinct macrophage subsets. We aimed to identify key new effectors that could control macrophage polarization and impact the development of cancer or colitis. Following treatment with the supernatants of tumor cells, macrophages showed an upregulation in *Fbxo38* expression. Subsequently, we further identified that FBXO38 promotes macrophage immunosuppressive function by upregulating the expression of M2-like genes via MAPK and IRF4 signaling without affecting M1-like macrophage polarization. Deletion of *Fbxo38* in macrophages was found to block tumor development and protect against DSS-induced colitis. Considering the distinct regulation of tumor development by FBXO38 in T cells and macrophages, we suggest that a comprehensive understanding of FBXO38 function in different cell types is critical for its further translational usage.

Keywords: FBXO38; Macrophage polarization; Tumor progression; Colitis

Cellular & Molecular Immunology (2023) 20:1367–1378; <https://doi.org/10.1038/s41423-023-01081-2>

INTRODUCTION

Immune cells within the tumor microenvironment (TME) play critical roles in tumor development and metastasis. Immunotherapies, including anti-PD-1/PD-L1 immune checkpoint blockade and adoptive cell therapies with CAR-T, TCR-T or NK cells, have achieved marked effects against cancer and prolonged patient survival. However, a large portion of cancer patients fail to benefit from anti-PD-1/PD-L1 blockade due to the complexity of TME components and immune cell subsets [1]. As the most abundant immune cells within the TME, tumor-associated macrophages (TAMs) can exhibit a wide spectrum of phenotypes that regulate tumor progression. In response to different stimuli *in vitro*, macrophages polarize into classically activated (M1-like) or alternatively activated (M2-like) subsets. M1-like macrophages are proinflammatory macrophages that activate T cells to kill tumor cells during the early stage of tumor onset [2]. In contrast, M2-like macrophages display immune suppressive functions that promote tumor cell proliferation or metastasis through various mechanisms [3–5].

Apart from their role in regulating tumor development, macrophages also play a crucial role in autoimmune diseases such as colitis and other diseases [6, 7]. For instance, in dextran sulfate sodium (DSS)-induced experimental colitis (inflammatory bowel disease, IBD) [8], M1-like macrophage-mediated inflammatory responses promote tissue damage [9], while M2-like macrophages contribute to inflammation resolution and tissue

repair [10, 11]. It is increasingly appreciated that targeting the key effectors of macrophage polarization to repolarize macrophages has therapeutic potential in cancer, autoimmune diseases and other diseases.

F-box only protein 38 (FBXO38, also known as HMN2D, MOKA, and SP329) is ubiquitously expressed in tissues and cells. Previous studies have elucidated that FBXO38 mutation results in familial distal spinal muscular atrophy (dSMA) [12, 13], and abnormal FBXO38 expression is associated with other diseases, such as chronic obstructive pulmonary disease (COPD) [14] and severe chronic periodontitis [15]. A recent study reported that FBXO38 is downregulated in tumor-infiltrating T cells and functions as an E3 ligase to mediate the degradation of PD-1; IL-2 treatment increases *Fbxo38* transcript levels, which downregulates PD-1 expression in T cells and enhances antitumor therapy [16]. PD-1 is also expressed in macrophages and mediates the development of cancer [17] and colitis [18]. However, the expression profile and function of FBXO38 in macrophages are unknown.

We analyzed the association between FBXO38 and different types of cancer using the Kplot and TCGA websites. Surprisingly, high vs. low levels of FBXO38 were both associated with longer survival depending on the type of cancer. We therefore investigated whether FBXO38 had differential functions in T cells and macrophages, leading to differences in the modulation of tumor development. In this study, we revealed that FBXO38 had no influence on M1-like macrophage polarization but promoted

¹School of Life Science, Hangzhou Institute for Advanced Study, University of Chinese Academy of Sciences, Hangzhou 310024, China. ²State Key Laboratory of Cell Biology, Shanghai Institute of Biochemistry and Cell Biology, Center for Excellence in Molecular Cell Science, Chinese Academy of Sciences, University of Chinese Academy of Sciences, Shanghai 200031, China. ³These authors contributed equally: Xin Zheng, Qi Jiang. ✉email: hongyanwang@sibcb.ac.cn

Received: 10 January 2023 Accepted: 27 August 2023

Published online: 12 October 2023

M2-like macrophage polarization. Furthermore, FBXO38 in macrophages promoted tumor development and protected against DSS-induced colitis.

MATERIALS AND METHODS

Mice

Fbxo38^{fllox/flox} mice were kindly provided by Dr. C. Xu (SIBCB, CAS). These mice were crossbred with *LysM^{Cre/−}* mice to generate cKO mice that specifically deleted FBXO38 in myeloid cells. The *Fbxo38^{fllox/flox} LysM^{−/−}* littermates were used as wild-type controls. The C57BL/6 mice used in this study were purchased from SLAC. Mice of the same age and sex were randomly allocated to experimental groups and maintained under specific pathogen-free (SPF) conditions in the institutional animal facility of the Center of Excellence in Molecular Cell Science (CEMCS), Chinese Academy of Sciences (CAS). Tumor sizes and body weight changes were monitored and kept within the allowable range established by the CEMCS IACUC.

Human PBMCs

Human PBMC samples were collected by the Shanghai Tenth People's Hospital of Tongji University. This study was approved by the ethics committee of the hospital. PBMCs were diluted with PBS and lymphocytes were isolated with Lymphocyte Separation Medium. The samples were centrifuged at 2000 rpm for 20 min in a swinging bucket rotor without braking. After performing density gradient centrifugation, the second layer containing the monocytes was carefully transferred to a new tube, washed with PBS, and centrifuged at 1200 rpm for 10 min. PBMCs were treated with 20 ng/ml GM-CSF in RPMI-1640 basic medium supplemented with 10% fetal bovine serum (FBS), 1% penicillin–streptomycin, and 1% L-glutamine for 6 days. Then, adherent human macrophages were stimulated with CM-MC38 for 48 h. Cells were resuspended in TRIzol reagent to extract RNA.

Cell culture

MC38 and Lewis lung carcinoma (LLC) cells were cultured in complete DMEM supplemented with 10% fetal bovine serum (FBS), 1% penicillin–streptomycin, and 1% L-glutamine. The culture supernatants were collected from the third-generation cells and filtered with a strainer (0.45 μm). The filtered supernatants were mixed at a 1:1 ratio with complete DMEM and named CM-LLC and CM-MC38. Peritoneal-elicited macrophages (PEMs) were harvested from mice on day 3 after 2.0 mL of 3% Brewer thioglycollate medium injection. Bone marrow cells were stimulated with M-CSF (20 ng/mL) for 7 days to generate BMDMs, as previously reported [19]. PEMs and BMDMs were maintained in complete DMEM supplemented with 10% (v/v) FBS, 1% penicillin–streptomycin (100 U/ml), and 1% L-glutamine at 37 °C with 5% CO₂ and were treated with IL-4/IL-13 (20 ng/mL) or CM-LLC and CM-MC38 for further analysis.

Cell proliferation assay

Sixteen to twenty-four hours before sampling, the thymidine deoxyriboside analog 5-ethynyl-2'-deoxyuridine (EdU) was administered by intraperitoneal injection (6.25 mg/kg) to tumor model mice. Single-cell suspensions were prepared from tumors and subjected to surface staining with anti-CD4 PerCP-Cyanine5.5 and anti-CD8a APC, followed by fixation with 4% PFA and 1% Triton for 15 min. Samples were then washed with PBS and added to the click reaction solution from the kit for 30 min so that EdU was labeled by Alexa Fluor 488. T-cell proliferation was analyzed by FACS.

CD8⁺ T cells were enriched from mouse spleens and immunostained with CFSE (5,6-carboxyfluorescein diacetate, succinimidyl ester), and were then cocultured with IL-4/IL-13-induced M2-like BMDMs at ratios of 1:1, 1:2, and 1:4. Samples were collected at 72 h, and T-cell proliferation was evaluated by measuring the levels of CFSE using FACS.

Mouse tumor model

A subcutaneous tumor model of MC38 was established in WT and cKO mice. After intraperitoneal injection of tribromoethanol (250 mg/kg), 5 × 10⁵ MC38 cells in 100 μl of PBS were subcutaneously inoculated into the right groin of the mice. Tumor size was measured every two days from day 7 using a microcaliper and calculated using the Formula $1/2 \times a \times b^2$ (a = length, b = width). Tumor growth curves were analyzed using Prism 8, and the mice were euthanized on day 19 for further analysis. The tumor tissue was minced and digested in complete DMEM (2% FBS, 1 mg/mL

collagenase IV, 0.2 mg/mL DNase I) at 37 °C for 1 h. The suspensions were then subjected to density gradient separation (40% and 70% Percoll, GE) followed by passing through a 70 μm strainer to collect immune cells. The cells were suspended in PBS containing 2% FBS and 1 mM EDTA for further analysis.

WT and cKO BMDMs were treated with IL-4/IL-13 for 24 h to polarize them into immunosuppressive macrophages. Then, they were cocultured with MC38 cells and injected into the groin of WT mice. MC38 cells (2 × 10⁵) were mixed with 4 × 10⁵ M2-like BMDMs in 100 μl of PBS and used to construct subcutaneous tumors in WT mice. Tumor volumes were recorded, and tumor growth curves were plotted starting on the seventh day. The mice were euthanized on the 21st day, and the tumors were removed and digested as described above.

A lung metastatic tumor model was constructed in WT and cKO mice by tail vein injection of B16 cells (8 × 10⁵) for 14 days. The mice were then euthanized, and the intact lungs were harvested, photographed, and weighed. A portion of the lung tissue was processed for immunostaining, and the remaining lung tissue was used to prepare a single-cell suspension, followed by flow cytometric analysis.

DSS-induced inflammatory bowel disease (IBD)

The DSS-induced IBD model was generated as previously described [7]. Briefly, paired male WT and cKO mice (8 weeks) were treated with water or 2% DSS (changed every 2 days). Weight loss was monitored daily to evaluate the severity of colitis, and DSS-containing water was fed to mice for 8 days followed by water for another 3 days. After measuring the colon length, the distal colon was cut into 2 mm pieces for paraffin embedding or for single-cell preparation. The intestinal segment was washed with Dissociation solution I (1 × PBS, 1 mM DTT, 10 mM HEPES) and II (1 × PBS, 30 mM EDTA, 10 mM HEPES) for 10 min separately. Samples were then digested in 1 × PBS with 2% FBS, 1 mg/mL collagenase IV (Sigma), and 0.2 mg/mL DNase I (Roche) for 90 min at 37 °C. After filtering through 70 μm filters, 2 × 10⁶ cells were used for flow analysis or for the isolation of F4/80⁺ macrophages.

RNA interference

PEMs were seeded in a 24-well plate (0.3 million cells/well) and transfected with siRNA (20 nM) using Lipofectamine 3000 (Invitrogen) following the manufacturer's instructions. After transfection with siRNAs targeting *Fbxo38*, *Irf4*, *Erk1/2*, and *p38*, knockdown efficiency was determined using qRT-PCR or western blot analysis. The siRNA sequences are listed in tables.

Western blotting analysis

PEMs and BMDMs were washed with PBS and lysed in lysis solution (50 mM Tris-HCl, 150 mM NaCl, 1% phosphatase inhibitor cocktail, 5 mM NaF, 2 mM NaVO₃, 1 mM PMSF, and 0.1% SDS). Cell lysates were boiled for 10 min at 100 °C, separated by SDS-PAGE, and electrotransferred to polyvinylidene fluoride (PVDF) membranes. The membranes were blocked for 1 h with 5% BSA or 5% milk, incubated with primary antibodies, washed three times with TBST, and then incubated with appropriate secondary antibodies. PVDF membranes were visualized using ECL plus reagents and an imaging analysis system.

qRT-PCR

For RNA extraction (Total RNA Extraction Reagent, Vazyme), the tissues were ground, and colon and tumor macrophages were isolated using biotin-labeled anti-F4/80 antibody and magnetic beads (EasySep Mouse Biotin Positive Selection Kit II). cDNA was generated using M-MLV transcriptase (Takara), dNTP mix (10 mM), and random primer (olig dN6). qRT-PCR was performed on a LightCycler 480 (Roche) using SYBR Green PCR Master Mix (Yeasen Biotech). β-actin was used as the housekeeping gene for normalization of the relative expression of target genes, and the fold change of each target gene was calculated using the $2^{-\Delta\Delta Ct}$ method. The sequences of all qRT-PCR primers are listed in tables.

Flow cytometry analysis

Spleen, thymus, and lymphoid tissues were ground and treated with red blood cell (RBC) lysis solution. All samples were blocked with anti-CD16/32 for 10 min, labeled with the indicated fluorescence-conjugated antibodies on ice in the dark for 40 min, and washed with FACS buffer (1 × PBS, 2% FBS, 1 mM EDTA, 1% P/S). After treatment with PMA, ionomycin, and monensin (4 h) and labeling of surface markers, cells were fixed with 4%

PFA for 15 min at room temperature, permeabilized with 0.1% Triton X-100, and stained with intracellular markers (IFN- γ , TNF- α , and Granzyme B) for 40 min at 4 °C. Samples were analyzed using a BD Fortessa flow cytometer and FlowJo software.

Histological and immunofluorescence analysis

The colons and tumors were fixed in 4% paraformaldehyde (PFA) overnight, embedded in paraffin, sectioned at 4- μ m-thick, deparaffinized and rehydrated, and stained with hematoxylin and eosin (H&E) solution. The tissue sections were evaluated using a BX51 light microscope (Olympus).

Tissue sections were also cooled to room temperature (RT) after 30 min of antigen retrieval, blocked with 1 \times PBS containing 3% donkey serum for 30 min, and incubated overnight with primary antibodies (Rat-F4/80, Mouse-ARG1) at 4 °C. The sections were washed three times with 1 \times PBS and incubated with secondary antibodies (Cy3-conjugated AffiniPure Donkey Anti-Rat IgG (H + L) and Alexa Fluor 647 AffiniPure Donkey Anti-Mouse IgG (H + L)) for 1 h at RT. Finally, the nuclei of the tissue sections were stained with DAPI for 10 min. The stained tissue sections were protected from light and photographed using a Leica TCS SP8 confocal microscope, and the data were analyzed using LAS_X_Small_3.0.2_16120_Setup software. The immunofluorescence intensity of ARG1 expressed in F4/80⁺ cells was quantified using ImageJ-pro 6.0.

RNA sequence analysis

PEMs were isolated from three pairs of WT and cKO littermate mice and stimulated with IL-4/IL-13 (20 ng/mL) for 24 h. Total RNA was extracted from cells using TRIzol. RNA quality was assessed using NanoDrop2000, and RNA integrity was determined using an Agilent Bioanalyzer 2100 (Agilent Technologies). RNA library construction and sequencing were performed at Majorbio. The raw counts were analyzed using DESeq2 software based on negative binomial distribution.

Quantifications and statistical analysis

All samples were strictly matched, and the sample sizes were large enough to ensure proper statistical analysis. Statistical analysis was performed using GraphPad Prism software, version 8. The unpaired *t* test, correlation analysis, one-way ANOVA, or two-way ANOVA test was used for statistical analysis. Ns denotes not significant ($p > 0.05$); * $p < 0.05$; ** $p < 0.01$; *** $p < 0.001$; **** $p < 0.0001$.

RESULTS

Different functions of FBXO38 in TAMs and T cells to control tumor development

As aberrantly altered gene expression and function are known to play a role in tumorigenesis, we conducted a study to investigate the expression of FBXO38 in different types of cancer using the Kaplan–Meier Plotter website. Our analysis revealed that high transcription of FBXO38 is associated with improved survival in patients with kidney renal clear cell carcinoma (KIRC) and lung adenocarcinoma (LUAD) (Fig. 1B). However, patients with gastric cancer (GC), stomach adenocarcinoma (STAD), and cervical squamous cell carcinoma (SCC) with low expression of FBXO38 had better survival (Fig. 1A). Moreover, we found that FBXO38 expression was altered in various tumors tissues compared to healthy tissues (Fig. S1A, B). These analyses demonstrated that there were correlations between FBXO38 expression and cancer.

Previous studies have reported that FBXO38 is downregulated and participates in tumor development by regulating the function of tumor-infiltrating T cells. We wondered whether FBXO38 is also downregulated and plays a role in TAM function regulation. To investigate this question, we treated peritoneal macrophages (PEMs) with culture medium from the MC38 tumor cell line (CM-MC38) to mimic the tumor microenvironment in vitro. Contrary to the downregulated *Fbxo38* in tumor-infiltrating T cells [16], *Fbxo38* transcription and protein levels were increased in PEMs after CM-MC38 treatment (Fig. 1C). We also treated human peripheral blood mononuclear cells (PBMCs) with GM-CSF to obtain human macrophages and observed a similar increase in *Fbxo38* expression levels after CM-MC38 treatment (Fig. 1D).

To further elucidate the function of FBXO38, we bred *Fbxo38* conditional knockout mice with *LysM^{Cre}* mice to generate myeloid cell-specific *Fbxo38* cKO mice (including macrophages) (Figs. S1C, 1E). Compared to wild-type (WT) mice, cKO mice showed normal body weight (Fig. S1D) and normal percentages of immune cell populations (Fig. S1E–H), including macrophages (CD11b⁺ F4/80⁺), T cells (CD4⁺ or/and CD8⁺), and B cells (B220⁺). We then injected MC38 cells into WT and cKO mice to generate subcutaneous tumors and found that cKO mice had significantly reduced tumor growth with smaller tumor volumes (Fig. 1F). Flow cytometry analysis (Fig. S2A) showed that the percentages and number of TAMs, as well as other tumor-infiltrating immune cells (Fig. S2B), were similar in WT and cKO mice. In addition, lung tumor models were constructed by intravenous injection of B16 cells, and cKO mice had attenuated tumor burden (Fig. 1G) with enhanced infiltration of immune cells (Fig. S2C, D).

FBXO38 promotes TAM immunosuppression in murine tumor models

FBXO38 was recently reported to promote the degradation of PD-1 in T cells. As TAMs can also express PD-1 to regulate tumor development [16, 17], we further analyzed PD-1 expression in macrophages but found no significant changes in MC38 subcutaneous tumors (Fig. 2A left) or B16-lung tumors (Fig. S3A) from WT and cKO mice. This finding may be due to the relatively low expression of PD-1 in macrophages. We then examined the expression of PD-L1, and found that PD-L1 expression levels were also comparable between WT and *Fbxo38*-deficient TAMs (Fig. 2A right). Our data indicate that *Fbxo38* expression in macrophages promotes tumor progression, which could explain the correlation of *Fbxo38* expression with patient survival in several types of cancer, such as gastric cancer, stomach adenocarcinoma and cervical squamous cell carcinoma. In contrast, a previous study showed that *Fbxo38* in T cells could decrease PD-1 expression levels to block tumor progression [16], which could explain the correlation of *Fbxo38* expression with patient survival in other types of cancers, such as kidney renal clear cell carcinoma and lung adenocarcinoma. These data suggest different functions of FBXO38 in immune cells, and cell type-specific targeting of FBXO38 should be considered for tumor immunotherapy.

Macrophages exhibit functional plasticity in response to different stimuli in the tumor microenvironment and can polarize toward a proinflammatory (M1-like) or immunosuppressive (M2-like) phenotype to differentially regulate tumor progression. To investigate the role of *Fbxo38* in macrophages, we determined the different gene signatures in WT or *Fbxo38*-deficient TAMs from MC38 subcutaneous tumors. The expression levels of proinflammatory cytokines, including *Il6*, *Il1b* and *Tnfa*, were comparable in WT and *Fbxo38* KO TAMs (Fig. 2B). However, the transcriptional levels of immunosuppressive genes, such as *Arg1*, *Arg2*, *Fizz1*, *Il10*, *Tgfb* and *Socs1*, were reduced in TAMs from cKO mice compared to those from WT mice (Figs. 2C and S3B). In addition, CD206 expression was downregulated and CD80 expression was upregulated in *Fbxo38* KO TAMs (Fig. 2D). These results suggest that *Fbxo38* promotes TAM polarization toward an M2-like phenotype, which could contribute to tumor progression.

To further investigate this possibility, we assessed the function of intratumoral T cells, as TAMs are known to modulate T-cell immunosurveillance. We analyzed tumor-infiltrating CD4⁺ T and CD8⁺ T cells from subcutaneous MC38 tumors in *Fbxo38* cKO mice and found that they indeed enhanced the production of IFN- γ (Fig. 2E) but did not affect TNF- α or Granzyme B levels (Fig. S3C). Similarly, CD8⁺ T cells from the lungs of B16-implanted cKO mice also produced higher levels of IFN- γ and TNF- α (Fig. S3D). To verify whether the immunosuppressive function of TAMs suppresses CD8⁺ T-cell proliferation, we examined the proliferation ability of CD8⁺ T cells in vivo and ex vivo. As expected, CD8⁺ T cells from the lungs of B16-implanted cKO mice demonstrated a greater proliferative ability with higher percentages of Ki67- and EdU-

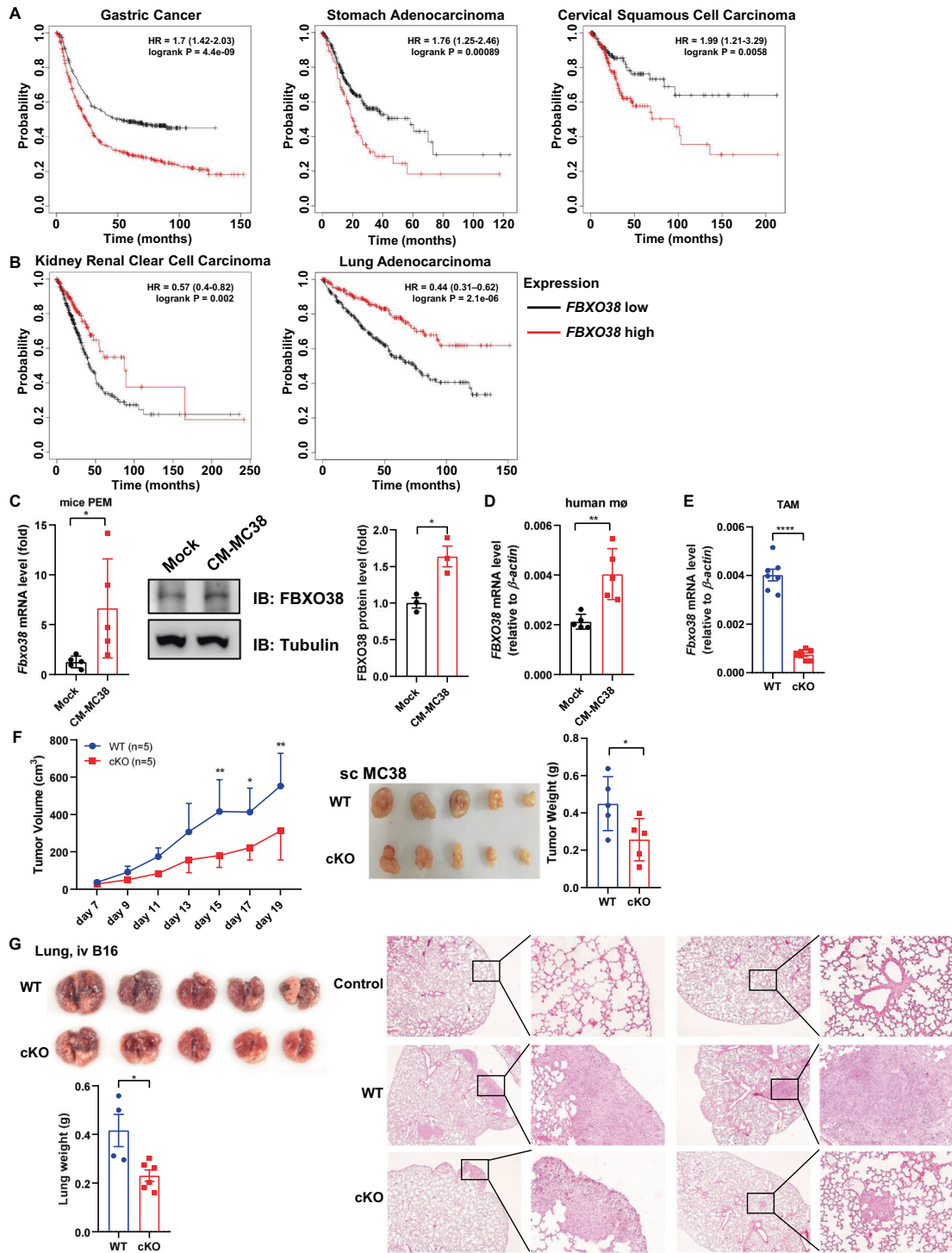


Fig. 1 Different functions of *FBXO38* in TAMs and T cells to control tumor development. **A, B** Analysis of the *FBXO38* transcriptional level and overall survival of patients with cancer from the Kaplan–Meier Plotter database. **C** Real-time quantitative reverse transcription PCR (qRT–PCR) (left panel, $n = 5$) and western blot analysis (middle and right panel, $n = 3$) of the expression of *FBXO38* in mouse PEMs with or without stimulation with CM-MC38 for 24 h. **D** qRT–PCR analysis of the transcription of *FBXO38* in induced human mφs (macrophages) ($n = 6$) with or without stimulation with CM-MC38 for 24 h. **E** qRT–PCR analysis of the transcription of *Fbxo38* in tumor-infiltrating macrophages (TAMs) from the subcutaneous MC38 tumors of WT and cKO mice. **F** Mean tumor volumes ($n = 5$) were calculated every two days from day 7 to day 19 (left panel). Representative picture ($n = 5$) (middle panel) and the weight ($n = 5$) (right panel) of tumors from WT and cKO mice subcutaneously inoculated with MC38 cells for 19 days. **G** Representative picture ($n = 5$) and the weight of lungs ($n > 4$) from WT and cKO mice at 14 days after the intravenous injection of B16 cells (left panel) and the corresponding H&E staining of the lungs from control and B16-implanted WT and cKO mice (right panel). Bar, 200 μm. Data information: ns, not significant; * $P < 0.05$; ** $P < 0.01$; using unpaired t test (**C** left and right panel, **D–F** right panel, **G** bottom panel) and two-way ANOVA with multiple comparisons (**F** left panel). Data were obtained from at least three independent experiments (**C** left and right panel, **D, E**) or are representative of three independent experiments (**C** middle panel, **F, G**). Error bars (**C–G**, mean \pm SEM)

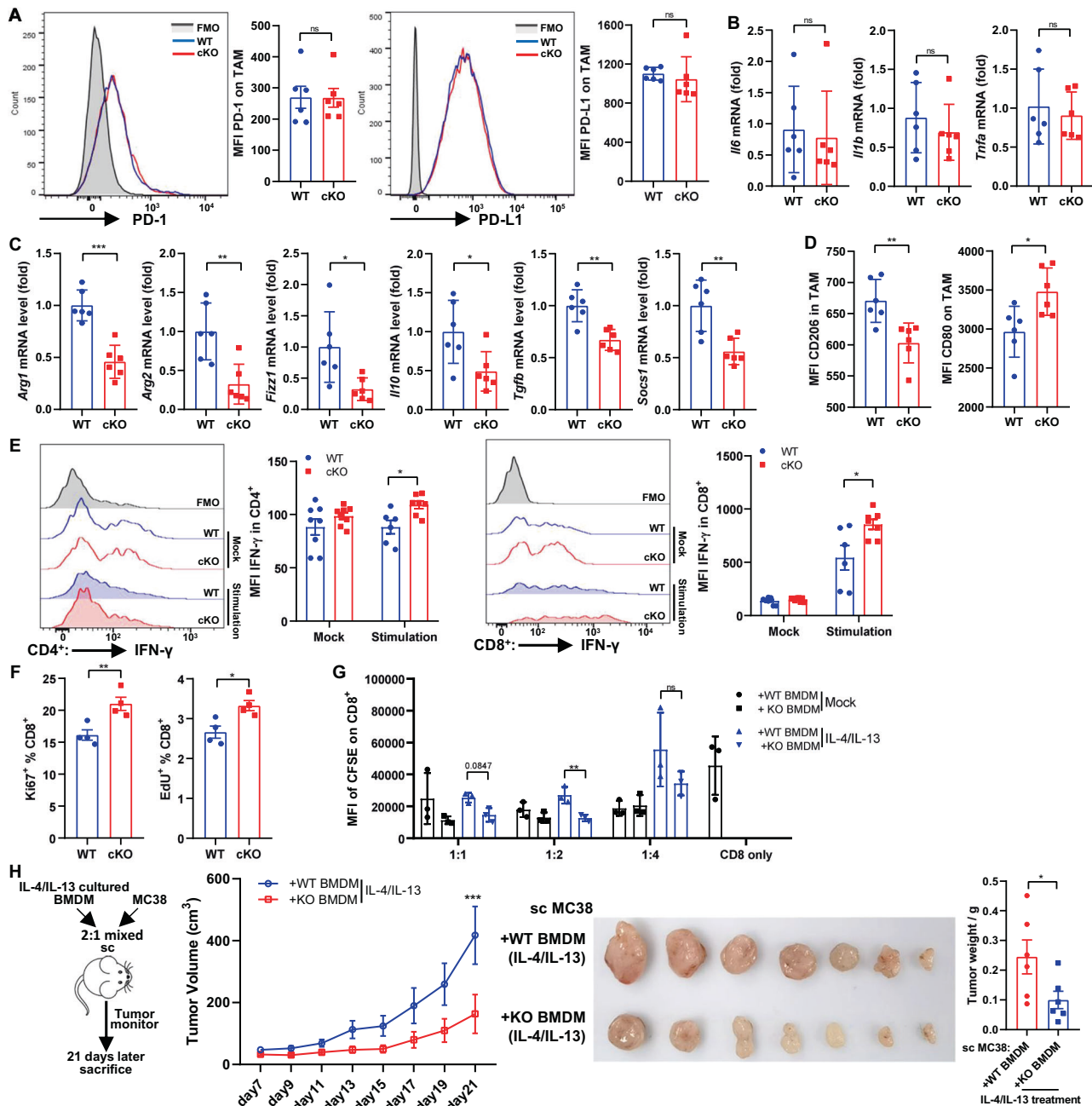


Fig. 2 FBXO38 promotes TAM immunosuppression in murine tumor models. **A** Representative flow cytometry histograms and mean fluorescence intensity (MFI) of PD-1 (left panel) and PD-L1 (right panel) ($n = 5$) in the TAMs of MC38 tumors. **B, C** TAMs were purified from WT ($n = 6$) and cKO ($n = 6$) mice by flow cytometry according to CD11b⁺ F4/80⁺, and then qRT-PCR was conducted to analyze the mRNA levels of the indicated genes. **D** Flow cytometry analysis of the MFI of CD206 and CD80 in TAMs ($n = 6$). **E** Representative flow cytometry plots showing the expression of IFN- γ in MC38 tumor-infiltrating CD4⁺ (left panel) and CD8⁺ (right panel) T cells. **F** Flow cytometry analysis of the percentage of Ki67⁺ (left panel) and EdU⁺ (right panel) positive CD8⁺ T cells in the lungs from B16 model mice. **G** Flow cytometric analysis of CFSE-labeled CD8⁺ T cells that were cocultured with BMDMs for 72 h, and WT or cKO BMDMs were pretreated with or without IL-4/IL-13 for 24 h. **H** Schematic diagram of the cell transfer experiment (first panel), and mean tumor volumes ($n = 6$) were calculated every two days from day 7 to day 19 (second panel). Representative picture ($n = 7$) (third panel) and the weight ($n = 6$) (right panel) of tumors from WT and cKO mice subcutaneously inoculated with MC38 cells for 19 days. Data information: ns, not significant; * $P < 0.05$; ** $P < 0.01$; *** $P < 0.001$; using unpaired t test (A–D, F, H right panel), two-way ANOVA with multiple comparisons (E, G, H second middle). Data are representative of two or three independent experiments (A–H). Error bars (A–H), mean \pm SEM.

positive cells (Figs. S3E and 2F). Furthermore, when cocultured with IL-4/IL-13-induced *Fbxo38*-deficient M2-like BMDMs ex vivo, CFSE-labeled CD3/CD28-activated CD8⁺ T cells showed better proliferation (Fig. 2G).

LysM^{Cre} mice can induce gene deficiency not only in macrophages but also in other myeloid cells. We found reduced *Fbxo38*

expression levels in the monocytes, granulocytes and dendritic cells (DCs) of *Fbxo38* cKO mice (Fig. S3F). To further confirm that *Fbxo38* promotes TAM immunosuppression to accelerate tumor progression, we mixed MC38 cells with IL-4/IL-13-induced M2-like BMDMs and subcutaneously inoculated them into wild-type mice (Fig. 2H left). Consistent with the data from cKO mice, we found

that when mixed with KO BMDMs, MC38 tumors grew slowly (Fig. 2H middle) and had smaller volumes (Fig. 2H right).

FBXO38 is positively correlated with immunosuppression in human samples

Upon analyzing the gene expression of healthy and tumor tissues in the TCGA database, we found that the expression of *FBXO38* showed a greater positive correlation with signature genes of M2-like macrophages (*MRC1*, *IL10*, *TGFB1* and *PPARG*) (Fig. 3A) than those of M1-like macrophages (*IL6*, *NOS2*, *IL23A*, *IL12A*) (Fig. S4A) in tumor tissues from patients with LUAD, STAD and liver hepatocellular carcinoma (LIHC). Furthermore, we verified the expression of genes related to immune regulation in clinical postoperative samples from patients with liver cancer. In human hepatocellular carcinoma tissue and tissues adjacent to cancer (par-cancer liver tissue, PCLT), *FBXO38* expression showed no correlation with *IL6* and *NOS2* in PCLT (Fig. S4B). However, it was positively correlated with the levels of M2-like macrophage signature genes, including *ARG1*, *MRC1*, *CEBPB* and *PPARG* (Fig. 3B).

Next, we prepared human macrophages with or without CM-MC38 treatment and determined the relationship between *FBXO38* and M2-like macrophage signature genes. Indeed, *FBXO38* mRNA levels were positively associated with *CD206*, *CEBPB* and *IL10* (Fig. 3C). Consistent with the data from tumor supernatant-treated human macrophages, we observed upregulated *FBXO38* expression in TAMs from human hepatocellular carcinoma (HCC) samples by single-cell sequencing analysis. Importantly, *FBXO38* expression was positively correlated with the levels of *FN1*, *MRC1*, *IL10RB*, *IL10*, and *CD206* in TAMs from human HCC tissue (Fig. 3D), which were previously reported as immunosuppressive genes [20]. These data indicate that *FBXO38* promotes macrophage immunosuppressive functions in both human and murine tumor models.

Fbxo38 in macrophages protects against IBD

Aside from tumors, macrophages and their plastic function play important roles in other diseases, including autoimmune diseases. To determine whether *Fbxo38* modulates macrophage polarization and immunosuppression in other diseases, we generated a DSS-induced IBD murine model. Comparing the severity of DSS-induced IBD, cKO mice exhibited much more severe weight loss (Fig. 4A) with shorter colonic length (Fig. 4B). Additionally, cKO mice had greater damage in colon histopathology, showing widely disrupted tissue architecture with increased mucosal hypertrophy and disappearance of intestinal crypts and goblet cells (Figs. 4C and S5A). Furthermore, the expression of immunosuppressive genes, including *Arg1*, *Arg2* and *Il10*, was downregulated in the colon tissues of cKO mice after DSS treatment, while the expression of proinflammatory genes, including *Il6*, *Nos2* and *Il1b*, was not affected (Fig. 4D). We also found comparable percentages of macrophages, monocytes and granulocytes in DSS-induced WT and cKO mice (Fig. S5B, C top). *Fbxo38* was mainly absent in macrophages (Fig. S5C bottom), and there were similar expression levels of PD-1, PD-L1, CD80, CD86 and MHC II on WT and *Fbxo38* KO macrophages (Fig. S5D).

To examine how *Fbxo38* deficiency affects macrophage polarization, F4/80⁺ macrophages were isolated from the colon of DSS-induced WT and cKO mice. *Fbxo38*-deficient macrophages reduced the mRNA levels of M2-associated genes (*Arg1*, *Arg2* and *Il10*) and did not affect the expression of M1-associated genes (*Il6* and *Il1b*) (Fig. 4E). In parallel with gene transcripts, the downregulated expression of ARG1 in F4/80⁺ macrophages was confirmed in the colon tissue of DSS-induced cKO mice by immunofluorescence staining (Figs. 4F and S5E).

We next used the published single-cell RNA-seq data of IBD patients [21] to analyze the expression of *FBXO38* and macrophage-related genes. Similar to our data from the murine IBD model, *FBXO38* exhibited a significant correlation with *IL10RA*,

IL10RB and *TGFB1* (M2-related genes) in the PBMCs from human IBD patients (Fig. 4G). Therefore, in both tumor and IBD models, we have elucidated that *Fbxo38* promotes macrophage immunosuppressive function without affecting proinflammatory macrophage polarization, resulting in tumor development but the alleviation of IBD.

Fbxo38 promotes IL-4/IL-13-induced M2-like macrophage polarization in vitro

To further investigate the function of *Fbxo38* in macrophage polarization, we used LPS/IFN- γ and IL-4/IL-13 to induce M1 and M2-like macrophages, respectively, in vitro. Consistent with our in vivo observation, knockdown (si*Fbxo38*, Fig. S6A) or KO of *Fbxo38* in PEMs did not alter the expression levels of M1-associated genes, including *Il6*, *Nos2*, *Il1b*, and *Tnfa* (Figs. S6B and 5A), but reduced the levels of M2-associated genes, including *Arg1*, *Fizz1*, *Ym1* and *Il10* (Figs. S6C and 5B).

Macrophages can also be induced from bone marrow and are termed BMDMs. After culturing bone marrow cells with M-CSF for 7 days, we found that the percentages of BMDMs (Fig. S6D, E) and the expression of *Adgre1* and *MerTK* (Fig. S6F) were not disturbed by *Fbxo38* deficiency. *Fbxo38* did not affect M1-BMDM polarization but was essential for the induction of M2-BMDMs (Fig. S6G).

Next, we treated WT and *Fbxo38* KO PEMs with supernatants from different tumor cell lines (named CM-MC38 and CM-LLC) to mimic the TME. Consistent with our above findings, *Fbxo38* KO PEMs did not affect the mRNA levels of *Il6* and *Il1b* but reduced the production of *Arg1* and *Il10* (Fig. 5C, D). Decreased protein levels of ARG1 were verified in *Fbxo38* KO PEMs upon treatment with IL-4/IL-13 or CM-LLC (Fig. 5E, F), but PD-1/PD-L1 expression (Fig. 5G) and phagocytic ability (Fig. S6H) were not significantly affected. Altogether, these results suggest that *Fbxo38* promotes M2-like macrophage polarization in vitro and enhances macrophage immunosuppression.

Fbxo38 affects macrophage polarization through MAPK and IRF4

During M2-like macrophage polarization, STAT6 and STAT3 are the key molecules that are phosphorylated and activated, inducing the expression of M2-related genes. However, we found that *Fbxo38* deficiency did not change the phosphorylation of STAT6 and STAT3 (Fig. S7A). Moreover, a STAT6-specific inhibitor (AS1517499) and a STAT3-specific inhibitor (Stattic) failed to reverse *Arg1* expression in IL-4/IL-13-treated *Fbxo38* KO macrophages (Fig. S7B).

To elucidate the underlying mechanism, we performed RNA-seq analysis of IL-4/IL-13-treated WT and *Fbxo38*-deficient PEMs. *Fbxo38*-deficient PEMs indeed had reduced expression level of M2-related genes, including *Arg1*, *Tgfb3*, and *Socs1* (Fig. 6A). Moreover, we observed that PI3K-Akt signaling and MAPK signaling were enriched pathways according to Kyoto Encyclopedia of Genes and Genomes (KEGG) signaling pathway analysis (Fig. 6B). Although previous reports suggest the key role of PI3K-Akt in macrophage polarization, the phosphorylation of PI3K, AKT and S6K was unchanged in *Fbxo38*-deficient PEMs (Figs. 6C and S7C, D). Notably, we found significantly decreased phosphorylation levels of ERK1/2 and p38, which belong to the MAPK signaling pathway, in *Fbxo38*-deficient PEMs (Figs. 6C and S7C, D). In agreement with these findings, we analyzed the RNA-Seq data and found that many MAPK pathway-related genes ($\log_2FC > 1$) were significantly changed in *Fbxo38* KO PEMs (Fig. 6D). In particular, the expression of *Mapk8ip3*, *Map3k12*, *EfnA5* and *Mapk9* was downregulated, which was confirmed by qRT-PCR (Fig. 6E).

We further investigated whether *FBXO38* affected the MAPK pathway to promote M2-like macrophage polarization. *Arg1* and *Fizz1* mRNA levels in IL-4/IL-13-treated *Fbxo38* KO PEMs were partially reduced by an ERK1/2 inhibitor (SCH772984) or a p38 inhibitor (BIRB796) alone but were substantially decreased to

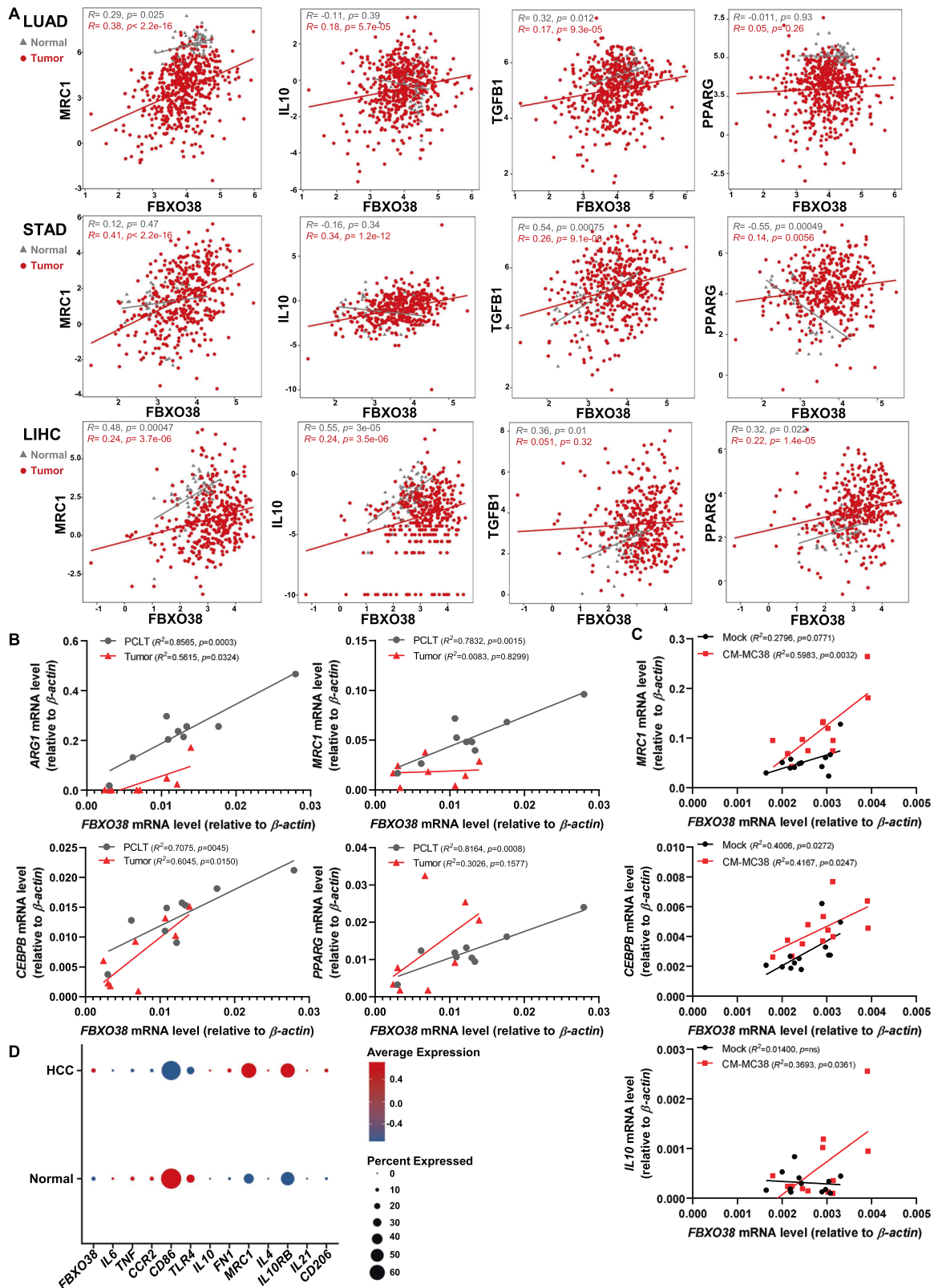


Fig. 3 FBXO38 is positively correlated with immunosuppression in human samples. **A** Correlation analyses of the transcriptional levels of the indicated genes with FBXO38 in normal (gray) or tumor (red) tissues from the TCGA database. **B** RT-PCR analysis of the mRNA expression of the indicated genes in hepatocellular carcinoma tissue ($n=9$) and PCLT ($n=9$). **C** Induced human macrophages ($n=12$) were treated with or without CM-MC38 for 48 h and analyzed for the mRNA levels of CD206, CEBPB, and IL10 by qRT-PCR. **D** Single-cell analysis of FBXO38 and related gene transcriptional levels in TAMs from HCC and normal tissues. Data information: ns, not significant; using correlation analyses (A–C). Data were pooled from three independent experiments (B, C)

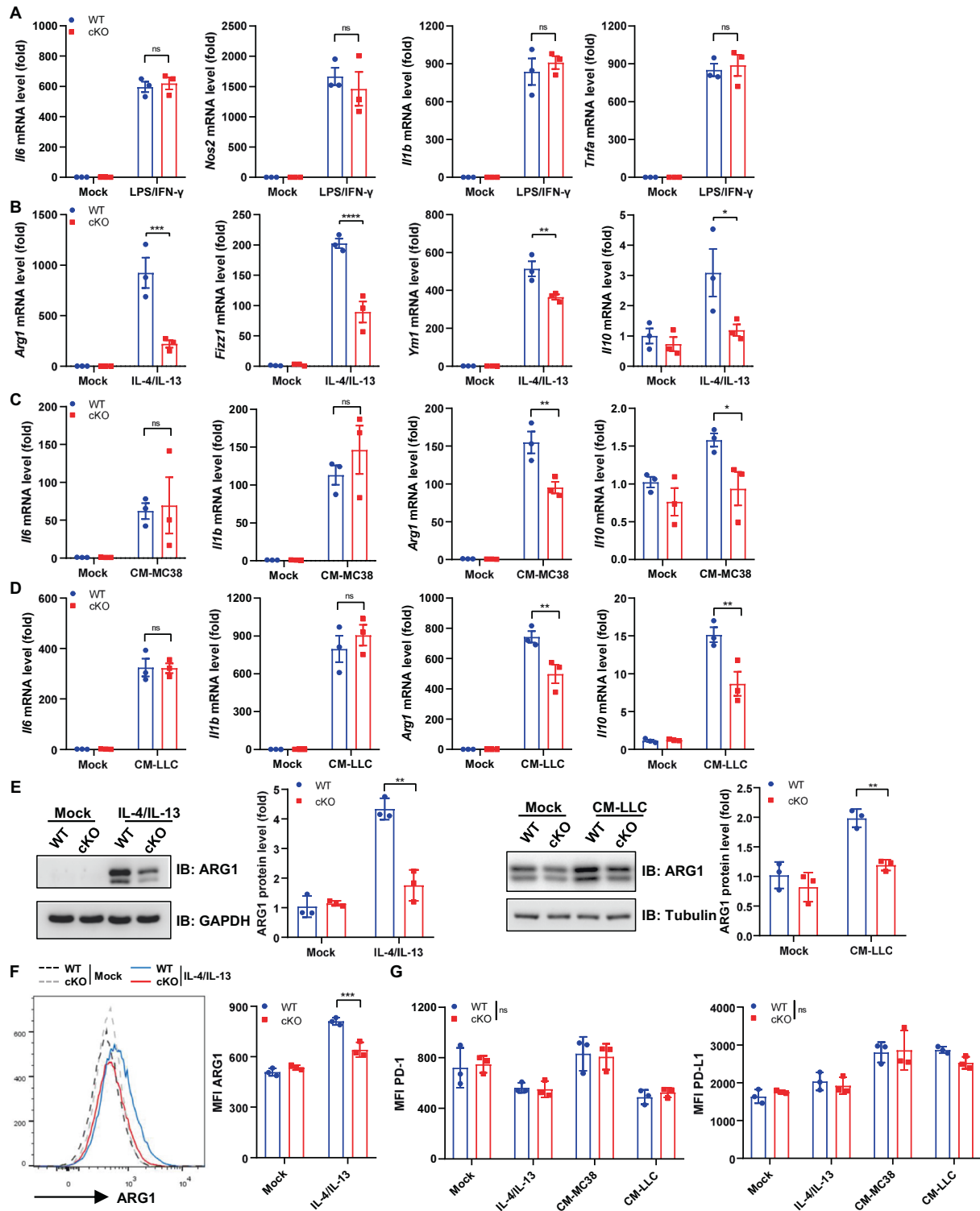


Fig. 5 *Fbxo38* promotes IL-4/IL-13-induced M2-like macrophage polarization in vitro. **A** The mRNA levels of *Il6*, *Nos2*, *Il1b*, and *Tnfa* were analyzed by qRT-PCR in the PEMs of WT ($n = 3$) and cKO ($n = 3$) mice after M1 polarization with LPS (100 ng/ml) and IFN- γ (20 ng/ml) for 3 h. **B** The mRNA levels of *Arg1*, *Fizz1*, *Ym1*, and *Il10* were analyzed by qRT-PCR in the PEMs of WT ($n = 3$) and cKO ($n = 3$) mice after M2 polarization with IL-4 (20 ng/ml) and IL-13 (20 ng/ml) for 24 h. **C**, **D** The expression of the indicated genes was analyzed by qRT-PCR in WT ($n = 3$) and cKO ($n = 3$) PEMs cultured with CM-MC38 (**C**) or CM-LLC (**D**) for 24 h. **E** The protein levels of ARG1, GAPDH, or tubulin were analyzed by immunoblot in WT and cKO PEMs after IL-4/IL-13 or CM-LLC treatment, and the statistics of ARG1 protein levels are shown. **F** Flow cytometry analysis showed the representative histograms and MFI ($n = 3$) of ARG1 in PEMs with or without IL-4/IL-13 stimulation for 24 h. **G** Flow cytometry analysis of PD-1 and PD-L1 MFI in IL-4/IL-13-, CM-MC38 and CM-LLC-treated WT ($n = 3$) or cKO ($n = 3$) PEMs. Data information: ns, not significant; * $P < 0.05$; ** $P < 0.01$; *** $P < 0.001$; **** $P < 0.0001$; using two-way ANOVA (**A–D**, **E** second and right panel, **F** right panel, and **G**). Data are from three independent experiments (**A–D**, **F** right panel, and **G**) or are representative of three independent experiments (**E** first and third panel, **F** left panel). Error bars (**A–D**, **E** second and right panel, **F** right panel and **G**, mean \pm SEM)

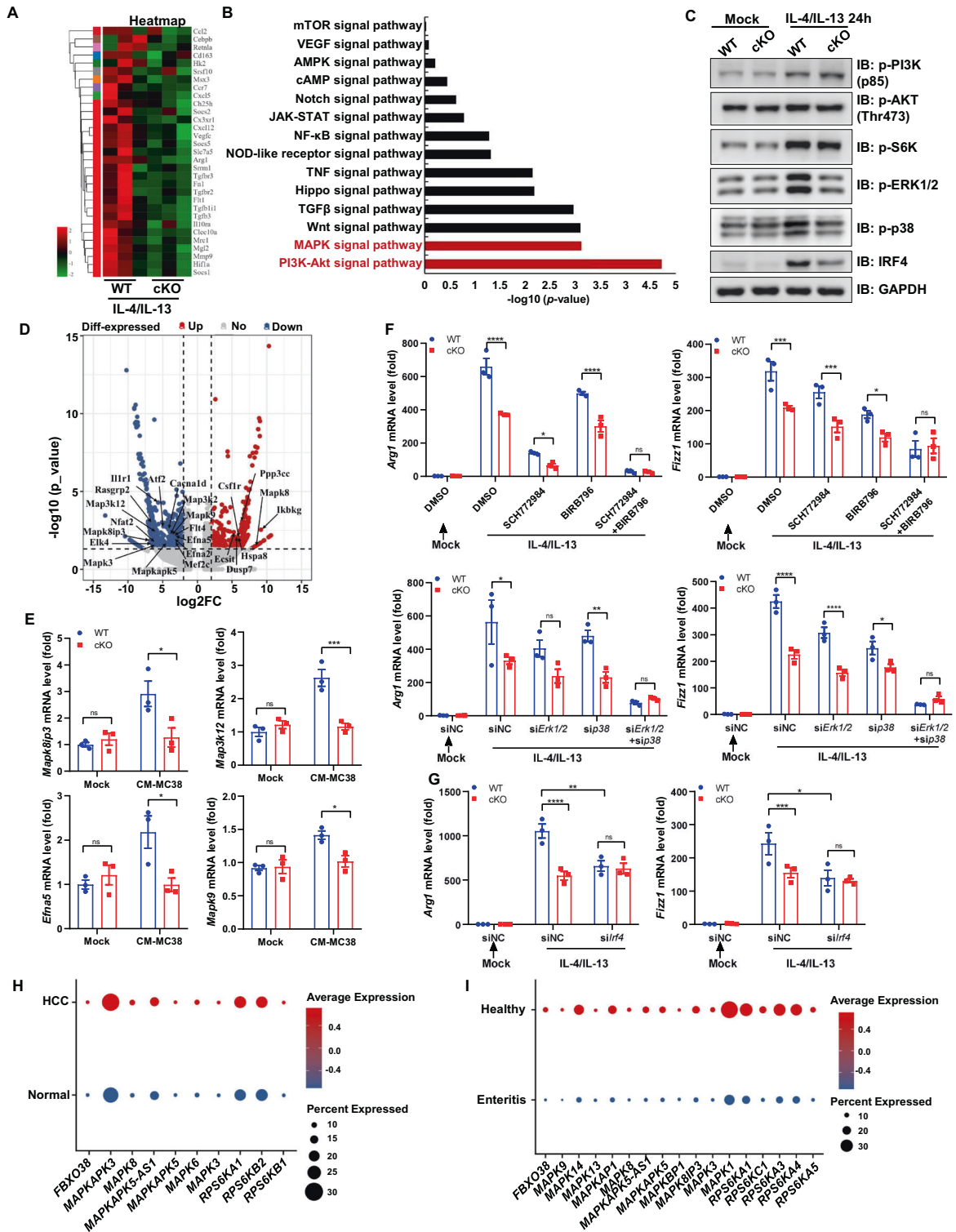


Fig. 6 FBXO38 affects macrophage polarization through MAPK and IRF4. **A** Heatmap showing the differentially expressed M2-related genes in IL-4/IL-13-stimulated WT ($n = 3$) and cKO ($n = 3$) PEMs by RNA-seq analysis. **B** KEGG pathway analysis was performed on the differentially expressed genes (DEGs) from the RNA-seq data of WT and cKO PEMs. **C** Immunoblot analysis was performed on IL-4/IL-13-stimulated WT and cKO PEMs using anti-p-PI3K, anti-p-AKT, anti-p-S6K, anti-p-ERK1/2, anti-p-p38, anti-IRF4, and anti-GAPDH antibodies, and the protein levels are shown in Figure S7D. **D** The differentially expressed genes ($\log_2 > 1$) in the MAPK signaling pathway were analyzed by RNA-seq. **E–G** The expression of the indicated genes was analyzed by qRT-PCR in WT ($n = 3$) and cKO ($n = 3$) PEMs pretreated with DMSO, SCH772984 (ERK1/2 inhibitor, 1 μM), or BIRB796 (p38 inhibitor, 0.2 μM) for 2 h (F top panel) or pretreated with the indicated siRNA (two siRNAs were used together) for 24 h (F bottom panel and H) and stimulated with CM-MC38 (E) or IL-4/IL-13 (F, G) for another 24 h. **H, I** The differentially expressed genes related to the MAPK signaling pathway in macrophages from human single-cell sequencing were analyzed. Data information: ns, not significant; * $P < 0.05$; ** $P < 0.01$; *** $P < 0.001$; **** $P < 0.0001$; using two-way ANOVA (E–G). Data are from three independent experiments (E–G) or are representative of three independent experiments (C). Error bars (E–G, mean \pm SEM)

levels similar to those in WT PEMs after the combined use of these inhibitors (Fig. 6F top). Next, siRNA against *Erk1/2* or *p38* was used (Fig. 5E, F). Consistently, knockdown of both *Erk1/2* and *p38* decreased *Arg1* and *Fizz1* expression levels in WT and *Fbxo38* KO PEMs to similar levels (Fig. 6F bottom). Importantly, using single-cell sequence data, we further confirmed the positive correlation of MAPK-related genes with *FBXO38* in macrophages from patient samples, including samples from patients with HCC (Fig. 6H) and enteritis (Fig. 6I).

IRF4 is a key transcription factor in M2 macrophages [22], and IRF4 expression is induced upon IL-4/IL-13 stimulation. We also found that in response to IL-4/IL-13 treatment, *Fbxo38* KO PEMs downregulated IRF4 expression (Fig. 6C). Moreover, siRNAs targeting *Irf4* (Fig. 57G) reduced *Arg1* and *Fizz1* expression levels in WT and *Fbxo38* KO PEMs to similar levels (Fig. 6G). Altogether, these data show that ERK1/2, p38 and IRF4 are downstream effectors of *FBXO38* that control M2-like macrophage polarization.

DISCUSSION

This study showed that the deletion of *Fbxo38* in myeloid cells did not affect the expression of PD-1 and PD-L1 on macrophages (Fig. 2A). In contrast, *Fbxo38* in T cells downregulated PD-1 expression to enhance T-cell-mediated elimination of tumors. It is worthy to point out that TAMs express PD-1 at much lower levels than tumor-infiltrating T cells. A previous study suggests that macrophages stimulated with IL-4/IL-13 for longer time could induce high PD-1 expression [23], which was observed by us in some experiments and in occasionally *FBXO38* deficiency might slightly enhance PD-1 levels. Further studies are needed to examine *FBXO38* functions in different macrophage subsets. Nevertheless, we found that *Fbxo38* in TAMs promotes tumor development by increasing the production of several immunosuppressive factors, including *Arg1*, *Il10*, and *Tgfb*. In addition, our analysis using the data from the Kplot website showed a negative correlation between *FBXO38* expression and patient survival time in patients with gastric cancer, stomach adenocarcinoma and cervical squamous cell carcinoma, while there was a positive correlation with patient survival time in patients with renal clear cell carcinoma and lung adenocarcinoma. One possible reason for this discrepancy might be related to the distinct function of *FBXO38* in different immune cells. This finding suggests that potential targets, including *FBXO38*, should be explored in multiple types of cells to evaluate their therapeutic benefits.

Furthermore, ARG1 and IL-10 were reported to promote tissue repair and limit inflammatory responses, and M2-like macrophages could provide protection against autoimmune diseases [24, 25]. In response to DSS-induced IBD, *Fbxo38* in myeloid cells protects the host against colitis by producing *Arg1*, *Il10* and other related factors (Fig. 4). Thus, maintaining *FBXO38* expression and function in myeloid cells could help protect against IBD.

We demonstrated that *Fbxo38* drives M2-like macrophage polarization without affecting M1-like macrophage polarization (Fig. 5). Previous studies have demonstrated that transcription factors such as STAT3, STAT6, C/EBP β and IRF4 can manipulate macrophage plasticity by upregulating M2-related genes, especially *Arg1*. Although the deletion of *Fbxo38* did not affect STAT3, STAT6 or PI3K/AKT activation in IL-4/IL-13-treated macrophages, we elucidated the important link between *FBXO38* and MAPK (Fig. 6). MAPK is a key kinase known to mediate the inflammatory response, and several studies have also reported that p38 and ERK1/2 are involved in the induction of M2-like macrophages [26–28]. *Fbxo38*-deficient macrophages showed reduced phosphorylation of ERK1/2 and p38, and knocking down ERK1/2 and p38 substantially reduced *Arg1* production to similar levels in WT and *Fbxo38*-KO macrophages (Fig. 6). Moreover, we found downregulated IRF4 expression in *Fbxo38* KO macrophages.

Interestingly, p38 activation is required for the upregulation of IRF4 expression in T cells from human psoriatic lesions [29]. This finding suggests that *FBXO38*, ERK1/2, p38 and IRF4 might work together in the same signaling pathway to promote M2-like macrophage polarization.

In summary, our study showed that *FBXO38* could promote MAPK activation and upregulate IRF4 expression to enhance macrophage immunosuppressive function, which differentially controls the development of cancer and IBD. Further studies might be needed to explore the function of *FBXO38* in tumor cells or in gut epithelial cells to evaluate the possibility of targeting *FBXO38* for the treatment of cancer or colitis.

DATA AVAILABILITY

The RNA sequencing data (GSE243182) and single-cell sequence analysis data [20, 21] (GSE125527, GSE140228) were deposited in the Gene Expression Omnibus. All other remaining data are available within the article and Supplementary Files or can be obtained from the corresponding author (HW) upon request.

REFERENCES

- Vesely MD, Zhang T, Chen L. Resistance mechanisms to anti-PD cancer immunotherapy. *Annu Rev Immunol*. 2022;40:45–74.
- Sica A, Erreni M, Allavena P, Porta C. Macrophage polarization in pathology. *Cell Mol Life Sci*. 2015;72:4111–26.
- Boutillier AJ, Elswa SF. Macrophage polarization states in the tumor micro-environment. *Int J Mol Sci*. 2021;22:6995.
- Noy R, Pollard JW. Tumor-associated macrophages: from mechanisms to therapy. *Immunity*. 2014;41:49–61.
- Zhang J, Shi Z, Xu X, Yu Z, Mi J. The influence of microenvironment on tumor immunotherapy. *FEBS J*. 2019;286:4160–75.
- Lin Y, Yang X, Yue W, Xu X, Li B, Zou L, et al. Chemerin aggravates DSS-induced colitis by suppressing M2 macrophage polarization. *Cell Mol Immunol*. 2014;11:355–66.
- Zhou X, Li W, Wang S, Zhang P, Wang Q, Xiao J, et al. YAP aggravates inflammatory bowel disease by regulating M1/M2 macrophage polarization and gut microbial homeostasis. *Cell Rep*. 2019;27:1176–89.e1175.
- Perse M, Cerar A. Dextran sodium sulphate colitis mouse model: traps and tricks. *J Biomed Biotechnol*. 2012;2012:718617.
- Zhao X, Di Q, Liu H, Quan J, Ling J, Zhao Z, et al. MEF2C promotes M1 macrophage polarization and Th1 responses. *Cell Mol Immunol*. 2022;19:540–53.
- Hunter MM, Wang A, Parhar KS, Johnston MJ, Van Rooijen N, Beck PL, et al. In vitro-derived alternatively activated macrophages reduce colonic inflammation in mice. *Gastroenterology*. 2010;138:1395–405.
- Weisser SB, Brugger HK, Voglmaier NS, McLarren KW, van Rooijen N, Sly LM. SHIP-deficient, alternatively activated macrophages protect mice during DSS-induced colitis. *J Leukoc Biol*. 2011;90:483–92.
- Sumner CJ, d'Ydewalle C, Wooley J, Fawcett KA, Hernandez D, Gardiner AR, et al. A dominant mutation in *FBXO38* causes distal spinal muscular atrophy with calf predominance. *Am J Hum Genet*. 2013;93:976–83.
- Akcimen F, Vural A, Durmus H, Cakar A, Houlden H, Parman YG, et al. A novel homozygous *FBXO38* variant causes an early-onset distal hereditary motor neuropathy type IID. *J Hum Genet*. 2019;64:1141–4.
- Saferali A, Yun JH, Parker MM, Sakornsakolpat P, Chase RP, Lamb A, et al. Analysis of genetically driven alternative splicing identifies *FBXO38* as a novel COPD susceptibility gene. *PLoS Genet*. 2019;15:e1008229.
- Shang D, Dong L, Zeng L, Yang R, Xu J, Wu Y, et al. Two-stage comprehensive evaluation of genetic susceptibility of common variants in *FBXO38*, *AP3B2* and *WHAMM* to severe chronic periodontitis. *Sci Rep*. 2015;5:17882.
- Meng X, Liu X, Guo X, Jiang S, Chen T, Hu Z, et al. *FBXO38* mediates PD-1 ubiquitination and regulates anti-tumour immunity of T cells. *Nature*. 2018;564:130–5.
- Gordon SR, Maute RL, Dulken BW, Hutter G, George BM, McCracken MN, et al. PD-1 expression by tumour-associated macrophages inhibits phagocytosis and tumour immunity. *Nature*. 2017;545:495–9.
- Wang Z, Hao C, Zhuang Q, Zhan B, Sun X, Huang J, et al. Excretory/secretory products from *trichinella spiralis* adult worms attenuated DSS-induced colitis in mice by driving PD-1-mediated M2 macrophage polarization. *Front Immunol*. 2020;11:563784.
- Zheng X, Xiao J, Jiang Q, Zheng L, Liu C, Dong C, et al. AKT2 reduces IFN β 1 production to modulate antiviral responses and systemic lupus erythematosus. *EMBO J*. 2022;41:e108016.

20. Zhang Q, He Y, Luo N, Patel SJ, Han Y, Gao R, et al. Landscape and Dynamics of Single Immune Cells in Hepatocellular Carcinoma. *Cell*. 2019;179:829–45.e20.
21. Boland BS, He Z, Tsai MS, Olvera JG, Omilusik KD, Duong HG, et al. Heterogeneity and clonal relationships of adaptive immune cells in ulcerative colitis revealed by single-cell analyses. *Sci Immunol*. 2020;5:eabb4432.
22. Satoh T, Takeuchi O, Vandenbon A, Yasuda K, Tanaka Y, Kumagai Y, et al. The Jmjd3-Irf4 axis regulates M2 macrophage polarization and host responses against helminth infection. *Nat Immunol*. 2010;11:936–44.
23. Antonsen KW, Hviid CVB, Hagensen MK, Sørensen BS, Møller HJ. Soluble PD-1 (sPD-1) is expressed in human macrophages. *Cell Immunol*. 2021;369:104435.
24. Grzywa TM, Sosnowska A, Matryba P, Rydzynska Z, Jasinski M, Nowis D, et al. Myeloid cell-derived arginase in cancer immune response. *Front Immunol*. 2020;11:938.
25. Oft M. IL-10: master switch from tumor-promoting inflammation to antitumor immunity. *Cancer Immunol Res*. 2014;2:194–9.
26. Zhang X, Fan L, Wu J, Xu H, Leung WY, Fu K, et al. Macrophage p38alpha promotes nutritional steatohepatitis through M1 polarization. *J Hepatol*. 2019;71:163–74.
27. Cheng Y, Zhu Y, Xu J, Yang M, Chen P, Xu W, et al. PKN2 in colon cancer cells inhibits M2 phenotype polarization of tumor-associated macrophages via regulating DUSP6-Erk1/2 pathway. *Mol Cancer*. 2018;17:13.
28. Jimenez-Garcia L, Herranz S, Luque A, Hortelano S. Critical role of p38 MAPK in IL-4-induced alternative activation of peritoneal macrophages. *Eur J Immunol*. 2015;45:273–86.
29. Alam MS, Gaida MM, Ogawa Y, Kolios AG, Lasitschka F, Ashwell JD. Counter-regulation of T cell effector function by differentially activated p38. *J Exp Med*. 2014;211:1257–70.

ACKNOWLEDGEMENTS

We thank Hangzhou Institute for Advanced Study and Center for Excellence in Molecular Cell Science, Chinese Academy of Sciences, University of Chinese Academy of Sciences. This work was supported by grants from the National Natural Science

Foundation of China (81825011, 32221002, 81930038 and 82303154), the Ministry of Science and Technology of China (2018YFA0800702), the Science and Technology Commission of Shanghai Municipality (22JC1403001, HS2021SHZX001) and the China Postdoctoral Science Foundation (2022M723141).

AUTHOR CONTRIBUTIONS

XZ and QJ performed the majority of the experiments and analyzed the data. MH, FY, MW, YQ, JW, MG and FH helped with the experiments. XZ, QJ and HW designed the study and wrote the paper.

COMPETING INTERESTS

The authors declare no competing interests.

ADDITIONAL INFORMATION

Supplementary information The online version contains supplementary material available at <https://doi.org/10.1038/s41423-023-01081-2>.

Correspondence and requests for materials should be addressed to Hongyan Wang.

Reprints and permission information is available at <http://www.nature.com/reprints>

Springer Nature or its licensor (e.g. a society or other partner) holds exclusive rights to this article under a publishing agreement with the author(s) or other rightsholder(s); author self-archiving of the accepted manuscript version of this article is solely governed by the terms of such publishing agreement and applicable law.